A New Distortion Solution for NIRC2 on the Keck II Telescope

M. Service[1], J. R. Lu[1], R. Campbell[2], B. N. Sitarski[3], A. M. Ghez[3], and J. Anderson[4]

[1] Institute for Astronomy, University of Hawai'i at Mānoa, Honolulu, HI 96822, USA
[2] W. M. Keck Observatory, Kamuela, HI 96743, USA
[3] University of California, Los Angeles, CA 90095-1547, USA
[4] Space Telescope Science Institute, Baltimore, MD 21218, USA

Abstract

We present a new geometric distortion model for the narrow-field mode of the near-infrared camera (NIRC2) fed by the adaptive optics system on the W. M. Keck II telescope. The adaptive optics system and NIRC2 camera were realigned on 2015 April 13. Observations of the crowded globular cluster, M53, were obtained before and after the realignment to characterize the geometric field distortion. The distorted NIRC2 positions of M53 stars were compared with precise astrometry of this cluster from *Hubble Space Telescope* observations. The resulting distortion map constructed just before the realignment is consistent with the previous solution derived using data from 2007 to 2009, indicating that the distortion has been stable to ∼0.5 mas. The distortion map changed significantly after a realignment of 4.5 mas (75%) rms, and the new distortion model for post-realignment observations have a total accuracy of ∼1.1 mas.

Key words: astrometry – instrumentation: adaptive optics

Online material: color figures

1. Introduction

High-precision astrometry is a powerful tool in astrophysics. Diffraction-limited imaging on 8–10 m class telescopes has been used to study the Galactic center (GC) in detail, including the discovery of the supermassive black hole and studies of its surrounding stellar population (e.g., Eckart & Genzel 1997; Ghez et al. 1998, 2005; Genzel et al. 2003; Paumard et al. 2006; Stolte et al. 2008; Bartko et al. 2009; Lu et al. 2009; Clarkson et al. 2012; Meyer et al. 2012; Yelda et al. 2014). A wide array of other science has similarly benefited, including measuring masses of stars and brown dwarfs from binary orbits (e.g., Konopacky et al. 2007; Liu et al. 2008; Dupuy et al. 2014), determining exoplanet orbits (Pueyo et al. 2015; De Rosa et al. 2015, e.g.), measuring masses and densities of small bodies in the solar system (e.g., Grundy et al. 2015), and studying compact objects (e.g., Cameron & Kulkarni 2007b; Rudy et al. 2015). The near-infrared camera, NIRC2, on the W. M. Keck II telescope (PI: K. Matthews) has been essential for a large number of these studies thanks to its stable and precise astrometry, yielding positional uncertainties as low as 0.15 mas (Lu 2008; Yelda et al. 2010).

Precise and accurate astrometry requires a thorough understanding of the imaging system used for observations. One limiting factor is knowledge of the geometric optical distortion in the imaging system. For example, uncorrected distortion in Galactic center imaging of the masers leaves >1 mas scale distortion (Yelda et al. 2010), which is at least a factor of 5–10 greater then the precision achieved with relative astrometry. In

general, these effects can be mitigated in crowded fields by using a large number of stars to transform individual exposures into a common astrometric reference frame. When the imaging system is stable, it is advantageous to measure the distortion and apply a distortion correction in the image analysis stage. Once the distortion is corrected, individual exposures can be stacked to increase sensitivity. Another advantage is that even sparse fields can be distortion corrected.

Distortions in NIRC2 were initially characterized using illuminated pinhole masks (Cameron & Kulkarni 2007a). However, the residual distortion in those solutions was still large compared to the relative astrometric error. On-sky data of M92 was used in Yelda et al. (2010) to measure the geometric distortion. The primary difference in these two approaches is the degree of systematic errors in the reference positions. In the case of the mask, reference position errors are set by how precisely the mask is manufactured. The on-sky experiment utilized *Hubble Space Telescope* (*HST*) data as the distortion-free external reference where the systematic noise is set by the residual distortion in that system. Currently, the distortion solution produced from on-sky data is more accurate (1.1 mas; Yelda et al. 2010) than the solution produced from pinhole mask observations (2–3 mas; Cameron & Kulkarni 2007a). A superior approach to distortion characterization would be to estimate the distortion-free reference positions from the observations themselves and dispense with the need for an external reference frame, as was done when deriving the *HST* distortion solution (Anderson & King 2006). However, this

requires observations with large translations at many orientations to constrain all high-order modes of distortion. The primary advantage of adopting an external reference is that we can measure the distortion of NIRC2 with a much smaller set of on-sky data as compared to the data set used to derive the *HST* distortion solution (Anderson & King 2006).

Previous work has demonstrated that the distortion of the NIRC2 system is stable over the period from 2007 to 2010 within the measurement errors for the solution (1.1 mas; Yelda et al. 2010). However, the Keck II adaptive optics (AO) system that feeds NIRC2 was realigned on 2015 April 13 to improve a long-standing issue of point-spread function elongation in 3–4 μm images. The source of this elongation was identified as the incorrect installation of the dichroic optic used to split between the infrared light passed to NIRC2 and the visible light used by the AO system. After the dichroic was adjusted to the correct orientation, further adjustments were needed to realign the optical axis while keeping aberrations minimized. A side effect of these improvements is a change in the geometric distortion of the system as seen by the instrument. This change requires new observations to characterize the geometric distortion of the new system.

In this work, we derive a new geometric distortion solution for the near-infrared camera (NIRC2) behind the Keck II adaptive optics (AO) system. We show that the distortion solution has changed by ∼4.5 mas (75%) rms after 2015 April 13 as a result of realignment work on the optical system. In Section 2, we describe NIRC2 and *HST* observations of the globular cluster M53 used to derive the new solution. Section 3 describes the data reduction and extraction of precise stellar positions. Section 4 describes how we use the stellar positions to fit distortion models for NIRC2 both before and after the system realignment. In Section 5, we derive errors and test both distortion solutions.

2. Observations

The first step in characterizing the geometric optical distortion in the NIRC2 camera is to measure stellar positions of a reference field. We use the dense globular cluster M53 as our reference field and derive reference positions using *HST*/ACS imaging(Section 2.1). The distortion in the *HST* images has been characterized and can be corrected to ≲0.5 mas (Anderson & King 2006). We then compare the nearly distortion-free reference positions to the distorted positions derived from NIRC2 imaging of the same field (Section 2.2). Our observations and methods mirror the process described in Yelda et al. (2010).

2.1. HST Observations of M53

M53 was observed with the *Hubble Space Telescope* on 2006 March 3 with ACS/WFC using the F814W filter. Five long (340 s) and one short (45 s) were taken centered on the
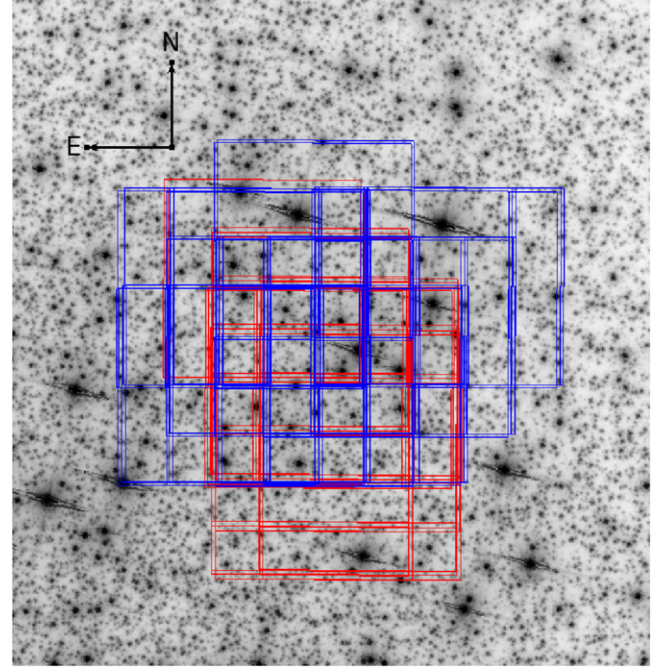
Figure 1. *HST* image of the M53 globular cluster, overlaid with NIRC2 pointings. The *HST* images were obtained with ACS/WFC in the F814W filter. Red boxes are NIRC2 observations taken in 2015 May. The blue boxes are NIRC2 observations from 2015 April. Each NIRC2 field is $10'' \times 10''$. (A color version of this figure is available in the online journal.)

M53 ($\alpha = 13^h12^m59^s$, $\delta = 18°10'18''$). The observations were taken with a position angle of $-104°.2$ and plate scale of 49.72 mas/pixel (van der Marel et al. 2007). These observations were part of the ACS Survey of Globular Clusters (GO-10775, PI: A. Sarajedini) and previously published in Anderson et al. (2008).

2.2. NIRC2 Observations of M53

M53 ($\alpha = 13^h12^m55^s$, $\delta = 19°10'8''.4$) was observed on 2015 April 2 UT and 2015 May 5 UT using the laser-guide star AO system on the W. M. Keck II 10 m telescope with the facility near-infrared camera NIRC2 (PI: K. Matthews). All observations were taken using the narrow-field camera ($10'' \times 10''$) and the K' filter ($\lambda_0 = 2.12\,\mu$m, $\Delta\lambda = 0.35\,\mu$m). We collected 133 science images in April and 100 science images in May with a total of 68 unique combinations of position angle (PA) and position offsets (Figure 1 and Table 1). The point-spread function delivered to the camera had an average FWHM of 55 mas and strehl ratio of 0.35. Based on spot checking the 10 brightest isolated ($dr > 10$ for any star within 2 magnitudes) sources in each image, we see that the typical variation in FWHM across the image is <3 mas with no coherent spatial structure.

To fully map the distortion solution, the scene of stars was dithered on the camera. This was done by dithering $2''.5$ in a square pattern from the central pointing and observed at two

Table 1
Summary of M53 Images

Date	PA (degrees)	Δ_x (pixels)	Δ_y (pixels)	N_{img}	t_{exp} (s)	Coadds	FHMW (mas)	Strehl	N_{stars}	σ_{pos} (pixels)
2015 April 2	0.0	0.0	0.0	4	5.0	10	64.3	0.27	76	0.072
	0.0	−15.9	−15.1	3	5.0	10	54.0	0.38	71	0.064
	0.0	18.1	1.6	4	5.0	10	69.8	0.22	62	0.064
	0.0	−16.0	3.9	4	5.0	10	53.9	0.37	117	0.086
	0.0	−251.6	−0.1	4	5.0	10	55.9	0.32	117	0.081
	0.0	−266.8	−16.8	4	5.0	10	64.3	0.23	88	0.081
	0.0	−230.4	0.4	4	5.0	10	60.9	0.26	98	0.086
	0.0	−266.7	1.5	4	5.0	10	60.9	0.28	95	0.074
	0.0	−502.6	−1.8	4	5.0	10	55.0	0.34	114	0.082
	0.0	−516.2	−17.9	4	5.0	10	57.7	0.29	105	0.086
	0.0	−482.7	2.6	4	5.0	10	53.0	0.36	123	0.091
	0.0	−516.2	1.7	4	5.0	10	56.3	0.32	86	0.090
	0.0	−747.6	−2.7	3	10.0	5	71.1	0.17	60	0.086
	0.0	−768.2	−18.6	2	10.0	5	56.4	0.31	131	0.060
	0.0	−730.6	0.0	3	10.0	5	56.6	0.30	133	0.067
	0.0	247.6	252.7	3	10.0	5	51.2	0.39	131	0.074
	0.0	230.7	236.4	3	10.0	5	50.2	0.45	148	0.083
	0.0	265.4	253.7	3	10.0	5	57.8	0.33	96	0.071
	0.0	−1.1	252.7	3	10.0	5	49.8	0.45	171	0.067
	0.0	−18.8	237.5	3	10.0	5	48.6	0.47	156	0.081
	0.0	17.1	253.8	3	10.0	5	52.3	0.37	152	0.073
	0.0	−251.3	252.2	3	10.0	5	52.4	0.37	160	0.071
	0.0	−269.0	236.0	3	10.0	5	54.7	0.33	138	0.070
	0.0	−232.0	253.7	3	10.0	5	50.0	0.43	178	0.065
	0.0	−501.5	250.7	3	10.0	5	55.1	0.33	114	0.067
	0.0	−518.4	234.8	3	10.0	5	52.3	0.41	175	0.077
	0.0	−485.1	252.5	3	10.0	5	53.0	0.36	168	0.076
	0.0	498.8	505.0	2	10.0	5	49.3	0.46	150	0.060
	0.0	480.8	490.0	2	10.0	5	47.9	0.49	161	0.058
	0.0	517.7	508.5	3	10.0	5	48.9	0.46	151	0.071
	0.0	246.7	506.0	2	10.0	5	51.7	0.35	121	0.060
	0.0	230.1	490.7	3	10.0	5	49.5	0.41	157	0.079
	0.0	264.9	508.5	3	10.0	5	48.2	0.43	176	0.081
	0.0	−505.8	501.7	3	10.0	5	58.4	0.28	68	0.091
	0.0	−524.2	485.9	3	10.0	5	58.2	0.25	85	0.081
	0.0	−486.5	504.4	3	10.0	5	52.0	0.31	110	0.073
	0.0	−775.0	485.2	2	10.0	5	57.4	0.33	126	0.062
	0.0	−738.8	502.4	3	10.0	5	58.9	0.30	116	0.094
	0.0	−258.5	752.3	3	10.0	5	58.5	0.31	111	0.089
	0.0	−274.9	736.6	3	10.0	5	61.2	0.32	115	0.093
2015 May 5	0.0	0.0	0.0	3	10.0	5	54.2	0.38	141	0.090
	0.0	−14.4	−16.0	4	10.0	5	64.9	0.23	75	0.009
	0.0	21.5	0.7	4	10.0	5	71.6	0.19	66	0.081
	0.0	−250.4	−1.9	4	10.0	5	68.6	0.19	72	0.100
	0.0	−265.6	−16.6	4	10.0	5	58.7	0.29	128	0.085
	0.0	−229.3	0.6	4	10.0	5	58.7	0.28	124	0.091
	90.0	1040.2	24.4	4	10.0	5	55.9	0.30	136	0.089
	90.0	1054.4	5.5	4	10.0	5	53.8	0.35	169	0.098
	90.0	1039.4	42.2	4	10.0	5	54.0	0.33	165	0.097
	90.0	1036.7	−224.4	3	10.0	5	50.5	0.27	127	0.079
	90.0	1054.3	−245.4	3	10.0	5	49.0	0.31	140	0.085
	90.0	1034.6	−199.2	3	10.0	5	48.2	0.31	129	0.091
	90.0	1037.2	−472.9	3	10.0	5	48.7	0.33	137	0.084
	90.0	1055.1	−495.0	3	10.0	5	47.7	0.34	142	0.081
	90.0	1034.5	−448.6	3	10.0	5	49.0	0.34	143	0.090
	90.0	789.1	276.2	3	10.0	5	53.0	0.34	155	0.087
	90.0	807.9	254.7	3	10.0	5	52.5	0.28	138	0.076
	90.0	786.2	300.6	3	10.0	5	51.6	0.30	153	0.077

Table 1
(Continued)

Date	PA (degrees)	Δ_x (pixels)	Δ_y (pixels)	N_{img}	t_{exp} (s)	Coadds	FHMW (mas)	Strehl	N_{stars}	σ_{pos} (pixels)
	90.0	788.4	26.2	3	10.0	5	54.1	0.30	160	0.082
	90.0	808.5	5.8	3	10.0	5	55.3	0.33	129	0.072
	90.0	789.2	50.1	3	10.0	5	58.7	0.26	119	0.33
	90.0	789.3	−222.5	3	10.0	5	59.6	0.28	122	0.088
	90.0	808.0	−244.2	3	10.0	5	64.9	0.19	79	0.068
	90.0	787.3	−196.6	3	10.0	5	59.5	0.26	129	0.085
	90.0	787.0	−472.7	3	10.0	5	51.7	0.39	153	0.089
	90.0	807.0	−495.3	3	10.0	5	55.1	0.34	134	0.090
	90.0	787.0	−449.5	3	10.0	5	61.2	0.29	106	0.090
	90.0	561.7	508.2	3	10.0	5	63.8	0.20	60	0.070
	90.0	541.3	551.8	3	10.0	5	65.2	0.25	78	0.088

different position angles. This is required to measure the distortion, as we need measurements of the same source at many locations on the detector. Additionally, this mitigates the effect of outlier stars (i.e., high proper motion) on the final solution. We take multiple exposures (2–4) at each pointing so that we can evaluate positional errors for each star prior to aligning the data to a global reference frame. The tip-tilt star used for these observations has R ∼ 13.5 and is 24″ west and 12″ south of the central pointing.

3. Data Reduction

The five *HST* images were reduced using the standard reduction pipeline and the resulting ∗_flt.fits files were downloaded 2015 September 5. We note that these images are not yet distortion corrected. The PSF fitting routines developed by J. Anderson (img2xym, xym2mat, xym2bar; see Anderson et al. 2008) were used to extract positions from individual flat-fielded images, correct distortion, and then collate the star lists to create a final stellar catalog from the *HST* images (Anderson & King 2006; Anderson 2007). Only stars detected in at least three images are included in the final catalog. We use this stellar catalog as our distortion-free reference frame.

The NIRC2 images were reduced and calibrated for high-precision astrometry using the methods described in Yelda et al. (2010). This involves background subtracting, flat fielding, cosmic-ray cleaning, and bad pixel masking. Typically, distortion would also be corrected at this stage; however, as we are deriving a new distortion solution, we do not apply these corrections. We also skip corrections for differential atmospheric refraction (DAR) as they require knowledge of the distortion solution. We will account for DAR when fitting the distortion model (Section 4). After reducing the images, the point-spread function (PSF) fitting routine *StarFinder* (Diolaiti et al. 2000) was used on each exposure. A correlation value of 0.8 was required to identify a stars in the images. *StarFinder* requires a set of PSF reference stars for each image. We

selected a set of bright stars using the *HST* catalog and then discarded stars that had secondary sources nearby ($\Delta(mag) < 4$ and $\Delta(r) < 0.\!''1$). Note that this step of source extraction assumes a single PSF for the entire image. A future analysis will combine an atmospheric and instrumental model to create a variable PSF for each image that accounts for anisoplanatism and field-dependent wavefront error, which should significantly improve on the the accuracy of this step. Systematic position offsets are caused by asymmetric variations in the shape of the image PSF with respect to the single empirical model PSF. The typical scatter of the eccentricity for bright isolated stars in these images is 0.08, which indicates there is true variation in each image, which is not captured in this analysis. These stars were then visually inspected in the NIRC2 imaging to ensure that they were bright and isolated in the NIRC2 images. For each exposure, a list of stellar positions and brightnesses was generated. Star lists for each dither position were produced by averaging position measurements from all images taken at that pointing (two to four images). Any stars that did not appear in at least two exposures was discarded. The rms errors from the combined star lists are used as the positional uncertainties (Figure 2). This gives us a NIRC2 stellar catalog with positions and errors for each pointing.

4. New Distortion Model

The NIRC2 narrow-field camera has a geometric distortion that was well characterized and shown to be static from 2007 to 2009 by Yelda et al. (2010). We have performed a similar analysis on the M53 data from 2015 both before and after the system realignment. Our approach consists of comparing on-sky NIRC2 observations to an external astrometric reference frame defined by high-precision *HST* observations of the same field. Several advances in the methodology are presented. Specifically, we use bivariate Legendre polynomials as the fitting basis for the model rather than spline surface interpolations. We also use an iterative approach to calculate the distortion correction required to
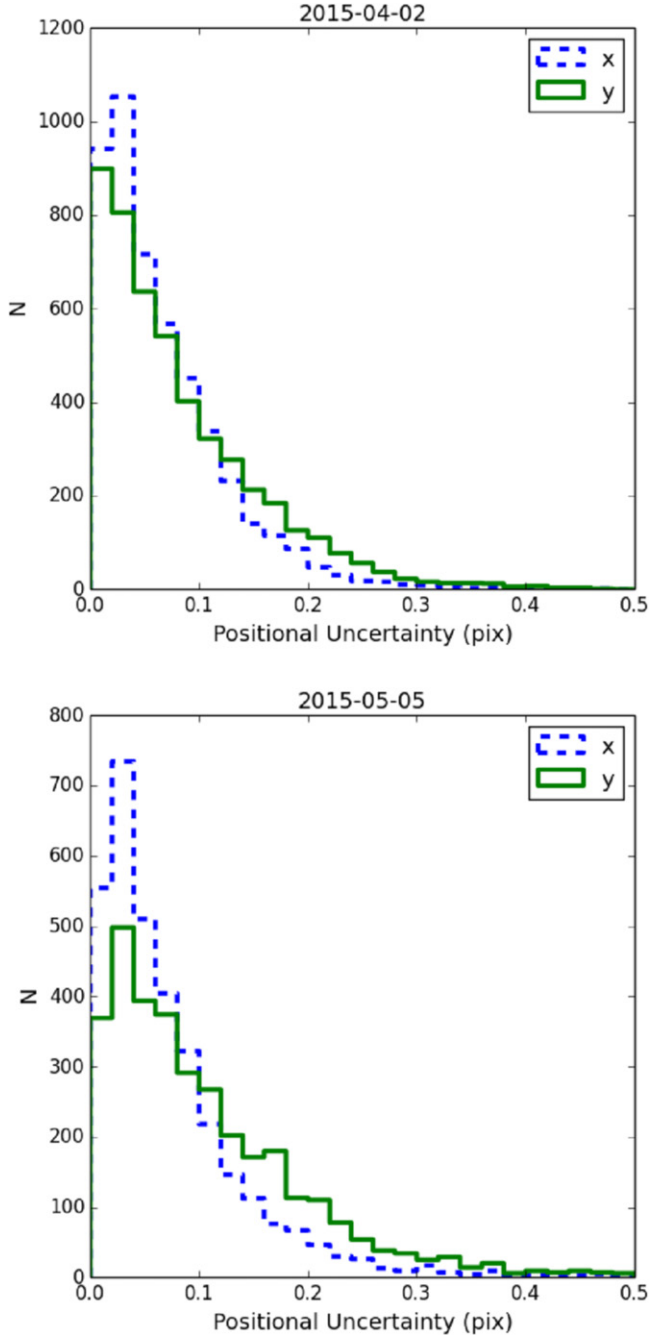
Figure 2. Positional uncertainties for all stars detected in the 2015-04-02 (top) and 2015-05-05 (bottom) data. These are the rms errors of the positions measured in all images taken at the same pointing. We include all of these stars in the subsequent analysis, and these errors are used to weight the fits of the geometric distortion (Figure 8).

(A color version of this figure is available in the online journal.)

transform NIRC2 measurements into a distortion-free reference frame. These methodology changes reduced the impact of proper motions between the NIRC2 and *HST* observations, which have a larger impact on our data due to the longer time difference

between observations (9 years versus 3 years). The changes also improved convergence when estimating the distortion. More details are presented below in a complete description of the analysis methods.

4.1. Constructing the Model

Two data sets are needed to fit a distortion model: stellar positions in a distortion-free frame (i.e., *HST* catalog) and measurements of the same stars at many positions on the NIRC2 detector. Before fitting for the distortion model, two preparatory steps are needed. We need to account for the differential atmospheric refraction (DAR) and transform the distortion-free coordinates into the reference frame of the NIRC2 camera. Ground-based images are compressed along the zenith direction due to DAR and the amount of compression changes with zenith angle. Fortunately, DAR is predictable with a model of the Earth's atmosphere and measurements of the ground temperature, pressure, and humidity (Gubler & Tytler 1998), which are all readily available from the Mauna Kea Weather Center.[5] Ideally, we would magnify the NIRC2 star lists along the zenith angle to correct for DAR; however, the true positions of the stars are distorted and cannot be directly corrected for DAR until a distortion solution is applied. Instead, we apply a compression to the *HST* positions as was done in Yelda et al. (2010). This compression is different for every NIRC2 image; thus, we produce a DAR-applied *HST* star list for each NIRC2 star list. We note that we only correct for achromatic DAR since the effect of chromatic DAR (<0.2 mas; Gubler & Tytler 1998) is smaller than the uncertainties in the *HST* ACS/WFC distortion solution (~ 0.5 mas) and can be neglected.

The final step before fitting is to transform the *HST* coordinates into a matched list associated with each NIRC2 catalog. This is accomplished using a four-parameter fit including plate scale, rotation, and positional offsets in two directions. The stars are matched if they are within 3 NIRC2 pixels of each other (~ 30 mas). All sources that have more than one match within the search radius are discarded. The NIRC2 and transformed *HST* positions are differenced to give $\vec{\delta}_{i,e}(x_{\mathrm{NIRC2}}, y_{\mathrm{NIRC2}})$ for each star, i, and each NIRC2 star lists, e, at the NIRC2 detector position (x_{NIRC2}, y_{NIRC2}). Figure 3 shows all the measured positional differences (a total of 4890 measurements in April and 3609 measurements in May). The April data set has more measurements due to the $\sim 30\%$ more images taken in that epoch. Large outliers due to mismatches or confusion are eliminated by clipping all 3σ outliers in both X and Y in 205×205 pixel bins, similar to Yelda et al. (2010). After clipping, there are 4779 measurements of $\vec{\delta}_{i,e}(x_{\mathrm{NIRC2}}, y_{\mathrm{NIRC2}})$ in April from 609 unique stars and 3336 measurements of $\vec{\delta}_{i,e}(x_{\mathrm{NIRC2}}, y_{\mathrm{NIRC2}})$ in May from 394 unique stars.
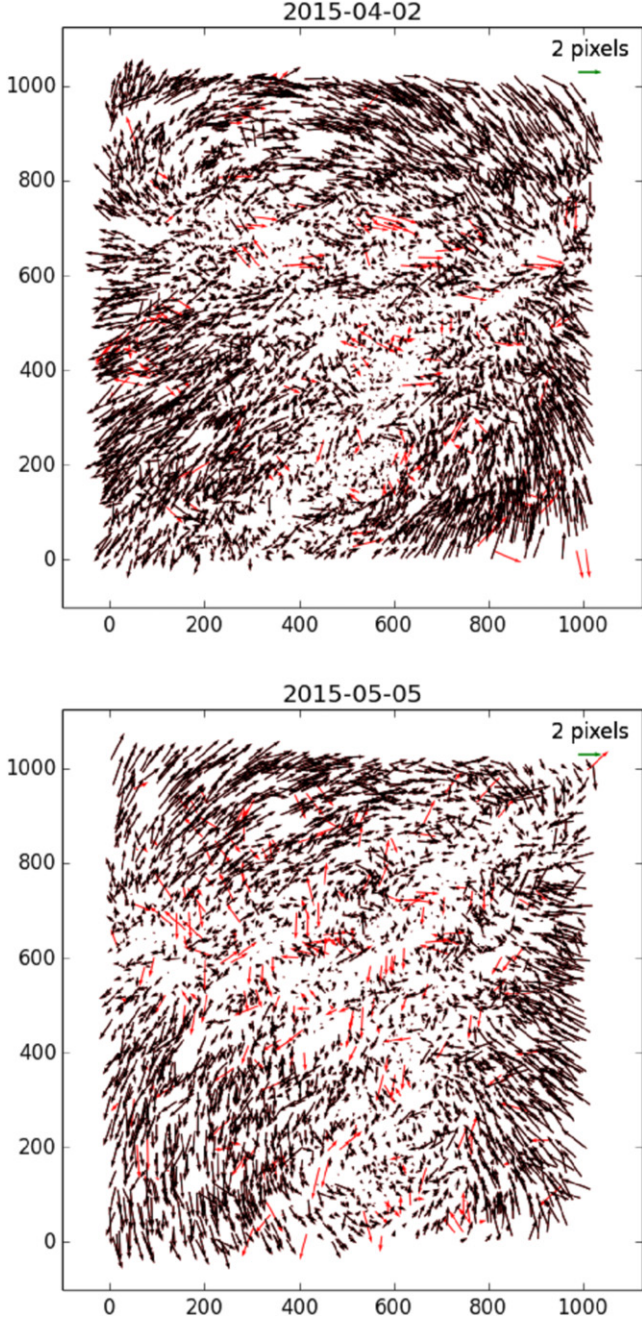
Figure 3. Observed positional differences between the *HST* and NIRC2 positions for the April (top) and May (bottom) data. Arrows in red are those rejected with sigma clipping. The change in distortion between the two data sets is clearly visible.

(A color version of this figure is available in the online journal.)

The maps of $\vec{\delta}_{i,e}(x_{\mathrm{NIRC2}}, y_{\mathrm{NIRC2}})$ are fit with multivariate Legendre polynomials independently for the April and May data sets. We chose this basis set over spline surface interpolations previously used because the Legendre polynomials are an orthogonal basis set, which provide faster and more reliable convergence in our fitting procedure. We also explored Cartesian polynomials and found that fit residuals were larger than for Legendre polynomials with the same number of free parameters. We fit independent polynomials to the deltas in each axis:

$$\delta x_{i,e} = T_e(x_{HST,i}) - x_{NIRC2,i,e} \qquad (1)$$

$$\delta x_{i,e} = a_0 + a_1 L_1(x)L_0(y) + a_2 L_0(x)L_1(y) \\ + a_3 L_2(x)L_0(y) + a_4 L_1(x)L_1(y) \; + ... \qquad (2)$$

where L_n are the nth Legendre polynomials, $x_{NIRC2,i,e}$ are the measured positions on the NIRC2 detector, $T_e(x_{HST,i})$ are the *HST* positions that were transformed (only rotation, scale, offsets, DAR) into the NIRC2 frame, and $[a_n]$ is the set of free parameters. Equivalent independent coefficients are fit for the Y axis. The fits are weighted by the positional uncertainties in both the *HST* and NIRC2 data using a least squares minimization of χ^2. We explored fitting with polynomials from the third to eighth order. A statistical comparison, using an F-test, shows the significance of improvement gained by going to a successively higher-order polynomials (Figure 4). A larger F value signifies greater improvement going from order M-1 $\rightarrow$ M, which makes it clear that at least a fourth-order polynomial is needed. We select a sixth-order polynomial for consistency as it most closely matches the Yelda et al. (2010) solution as measured by the average deviation over the entire NIRC2 detector. We note that this first fit does not account for the motion of the stars between 2006 and 2015.

4.2. Iterative Procedure

Inaccuracies in the reference frame positions of stars due to proper motions, residual distortion in the *HST* reference frame (0.5 mas), and any other large residual between the two instruments, can lead to larger errors in the final distortion solution. Any global motion or rotation of the stars in the M53 cluster will be removed by the four-parameter transformations (2D translation, scale, rotation). However, the internal motions of stars in the cluster will shift individual stars with respect to each other. Most of the stars in our field of view are members of M53 globular cluster. The predicted velocity dispersion is 0.066 mas/yr in the plane of the sky given the measured line-of-sight velocity dispersion (5.6 km s^{-1}; Kimmig et al. 2015) and distance of 17.8 kpc (Kharchenko et al. 2013). This means that we expect offsets due to relative motion to appear at the $\sim$0.6 mas level due to the nine-year time baseline. To mitigate the effects of these offsets, we adopt an iterative scheme that redefines the reference positions based on the NIRC2 data and an initial distortion solution.

We adopt an iterative approach to fitting the distortion solution and then improving the reference frame in order to mitigate the effects of systematic errors in the reference frame positions. We apply the first distortion solution to the NIRC2 catalogs and then create a new reference frame by averaging all
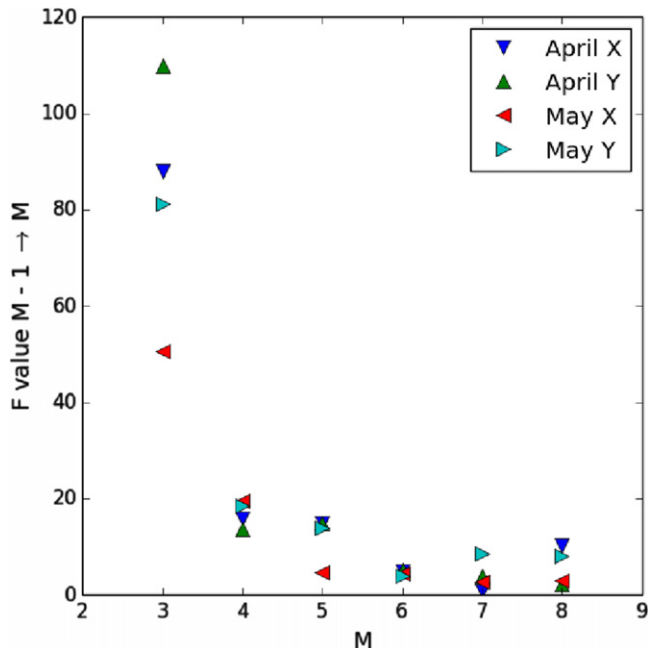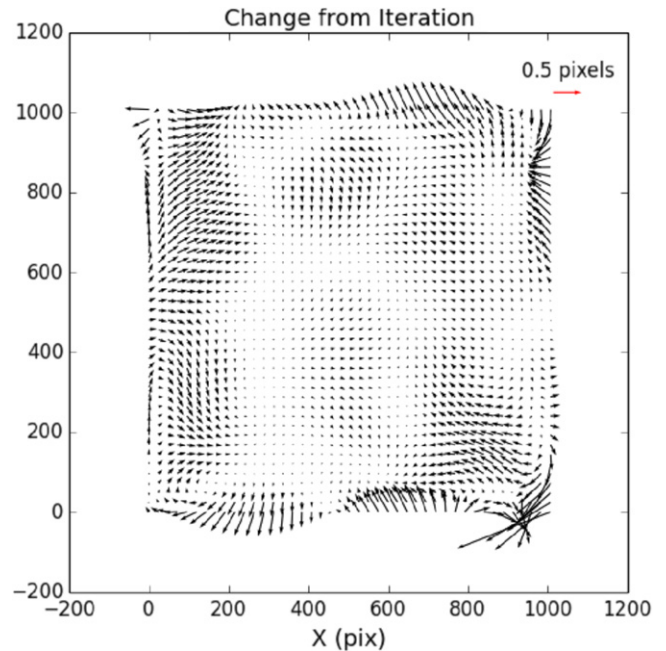
Figure 4. F values for all fitting orders tested. A higher value corresponds to a more significant improvement of the fit quality. There is significant improvement from going to at least fourth order, however, beyond that the gains are quite small.

(A color version of this figure is available in the online journal.)

Figure 5. Change in the distortion model between the first and the final iteration for the 2015-05-05 data. We note that the average absolute value of the change is less than 0.9 mas, which is less than the total error in our solution.

(A color version of this figure is available in the online journal.)

position measurements for each star. In detail, the individual exposures are first distortion corrected. Then, each exposure is transformed into a common reference frame using a four-parameter fit (i.e., angle, scale, x offset, y offset) of the transformation between the individual NIRC2 catalogs and the *HST* reference. The distortion-corrected, transformed star lists are then averaged together to make a new reference frame is used in place of the *HST* measurements as the distortion-free frame. The fitting procedure is then repeated until the residual difference between the derived distortion solutions in successive passes is less than .05 mas (six iterations). The total change in the distortion solution between the first fit and the final fit shows how the proper motions were affecting the fit (Figure 5). The average absolute value of the residual is <1.0 mas, which is at the same level as the total uncertainty in the distortion model. Areas on the detector with the largest change in the iterative process correspond to the areas with the largest fitting errors, especially at the edge of the detector.

4.3. Uncertainty in the Distortion Model

The uncertainty in the distortion model fit is estimated using a half-sample bootstrap method. For each of 100 trials, we randomly sample half of the data with replacement of the measurements and repeat the entire fitting process for both the

April and May data. The half-sample is selected prior to the sigma clipping. The fitting procedure (including clipping) produces 100 different distortion lookup tables, and we adopt the rms scatter at each pixel as the fitting error in that pixel. Figures 6 and 7 show the fitting error for both solutions. The 2015-05-05 solution has mean fitting errors of 0.53 mas and 0.54 mas in X and Y, respectively.

5. Results

Our main results are the distortion solutions shown in Figure 8 and their associated errors (Figures 6 and 7). These are lookup tables generated by evaluating the fits from the previous section at the center of every pixel on the NIRC2 detector and are the values that should be added to raw NIRC2 positions to shift them to a distortion-free frame. We also find that the distortion changed by ~4.5 mas rms due to the realignment of the AO bench.

5.1. Distortion Stability Prior to Realignment in 2015 April

The simplest test of our method is to verify that our April (pre-realignment) solution agrees with the previous solution. Figure 9 shows the differences between the solutions divided by the errors summed in quadrature. More than 90% of the pixels agree within 1σ; therefore, we measure no statistically

2015-04-02 Uncertainty

2015-05-05 Uncertainty
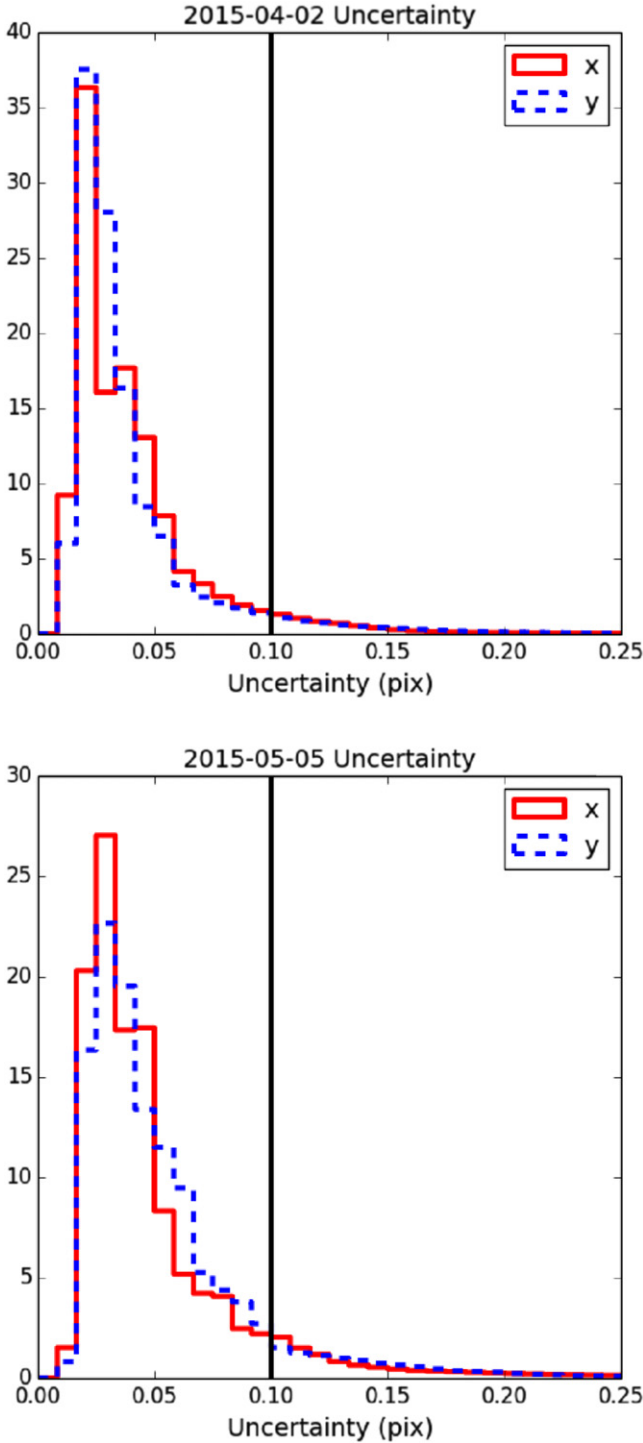
Figure 6. Fitting errors in the distortion solutions for 2015-04-02 (top) and 2015-05-05 (bottom). The vertical line indicates the residual distortion in the solutions. The distribution of uncertainties for all pixels in the distortion model lookup table yield a mean uncertainty for the 2015-04-02 model of 0.42 mas in both X and Y. The 2015-05-05 solution has mean uncertainties of 0.53 mas in X and 0.55 mas in Y.

(A color version of this figure is available in the online journal.)

significant differences between the Yelda et al. (2010) solution using imaging data from 2007 to 2009 and our pre-realignment solution. This verifies our method and confirms that the distortion seen by the NIRC2 camera is stable. To confirm that the residual distortion in the two solutions are equivalent, we use our new fit to analyze two high-precision Galactic center data sets taken on 2007 May 17 and May 20. These data sets are of the central field around the Galactic center taken at a PA of $0°$ and PA of $200°$ at approximately the same central pointing (Yelda et al. 2010, Section 3.2). We can use this data to measure the average residual distortion in the solution by comparing the measured positions of a single object at two different locations on the detector. The PA of $200°$ are transformed into the PA of $0°$ reference frame using a four-parameter fit and then the average residual distortion is calculated using the differences between the stellar position measurements:

$$\sigma_x = \sqrt{\frac{1}{2}\sum_i^{N_{stars}}\frac{(\Delta_{x,i} - \langle\Delta_x\rangle)^2}{(N_{stars} - 1)} - \frac{1}{2}(\sigma^2_{pos,0°} + \sigma^2_{pos,200°})} . \quad (3)$$

Here, N_{stars} is the number of stars matched between the two data sets, and $\sigma_{pos,0°}$ and $\sigma_{pos,200°}$ are the positional uncertainties for stars brighter than the K magnitude of 14.5. We subtract the average positional uncertainties as they also contribute to the scatter ($\sigma_{0°} \sim 0.13$ mas, $\sigma_{0°} \sim 0.17$ mas). This results in an estimate of the average residual distortion in our new pre-realignment solution of 1.2 mas in X and 1.0 mas in Y. We can subtract the fitting error to find that our total unaccounted for residual distortion is 0.9 and 1.1 mas for X and Y, respectively, in the 2015-04-02 solution. This is comparable to the measured final residual of the Yelda et al. (2010) solution, which is 1.1 and 1.0 mas for X and Y, respectively. The extra systematic error is added in quadrature with the bootstrapped fitting errors to produce the final error maps for the new solution.

5.2. Quality of New 2015 May Distortion Solution

Unfortunately, we lack a similar independent (non-M53) two-PA data set to test the post-realignment solution as was used in Yelda et al. (2010) and the previous section. Instead, we apply our new (2015-05-05) solution to the May M53 NIRC2 imaging data. This is accomplished using *Drizzle* (Fruchter & Hook 2002). We then use *StarFinder* to extract positions from the individual corrected images and create a stack of position measurements for each star from all the available images. A four-parameter transformation is used to map the catalogs to the common *HST* reference so they can be averaged. We adopt the mean scatter in the measured stellar positions as representative of the residual distortion in the solution. The mean rms scatter in the May position measurements for the 60 stars measured in at least 20 individual images is 1.1 mas in both X and Y. This 1.1 mas is the total error due to the combination of individual positional errors
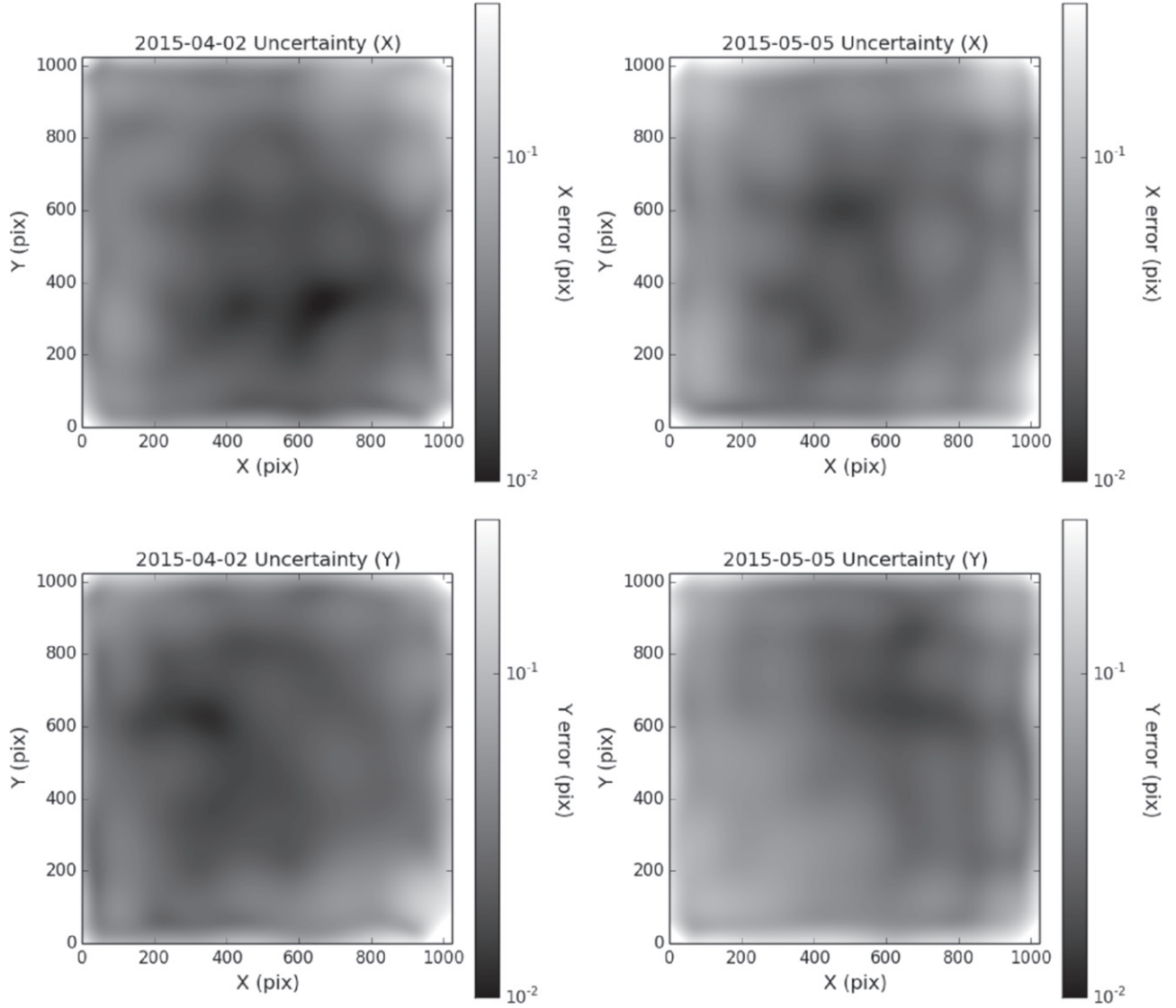
Figure 7. Fitting errors in the distortion solutions for 2015-04-02 (left) and 2015-05-05 (right) shown with log stretch. Spatial maps of the errors are shown for both the X (top) and Y (bottom) directions. The largest uncertainties are at the corners of the detector. The distribution of uncertainties for all pixels in the distortion model lookup table yield a mean uncertainty for the 2015-04-02 model of 0.42 mas in both X and Y. The 2015-05-05 solution has mean uncertainties of 0.53 mas in X and 0.55 mas in Y. Note that an additional error of 1.0 mas must be added to the 2015-05-05 solution to fully describe the distortion measurement error.

(Figure 2), the fitting errors (Figure 7), and the residual distortion. We subtract the average positional and fitting errors in quadrature, which leaves 1.0 mas of residual distortion in the solution. Note that the total accuracy of the solution is the addition in quadrature of the residual distortion (1.0 mas) and the fitting error that varies across the detector. One source of this systematic error is PSF variability across the images frames, which will be addressed in a future analysis.

As a final consistency check, we compare the distortion-corrected positions from the April data to that of the May data. We only include stars detected in at least three images in both data sets, which gives a total of 247 stars. We expect that the differences between the two positions should be consistent within the uncertainties of both solutions. The mean rms deviation is 1.1 mas for both x and y, which is consistent within the uncertainties of the individual distortion solutions (~1.1 mas)

5.3. Changes in Plate Scale

The same matching of distortion-corrected NIRC2 positions to the *HST* positions can also be used to to calculate the global
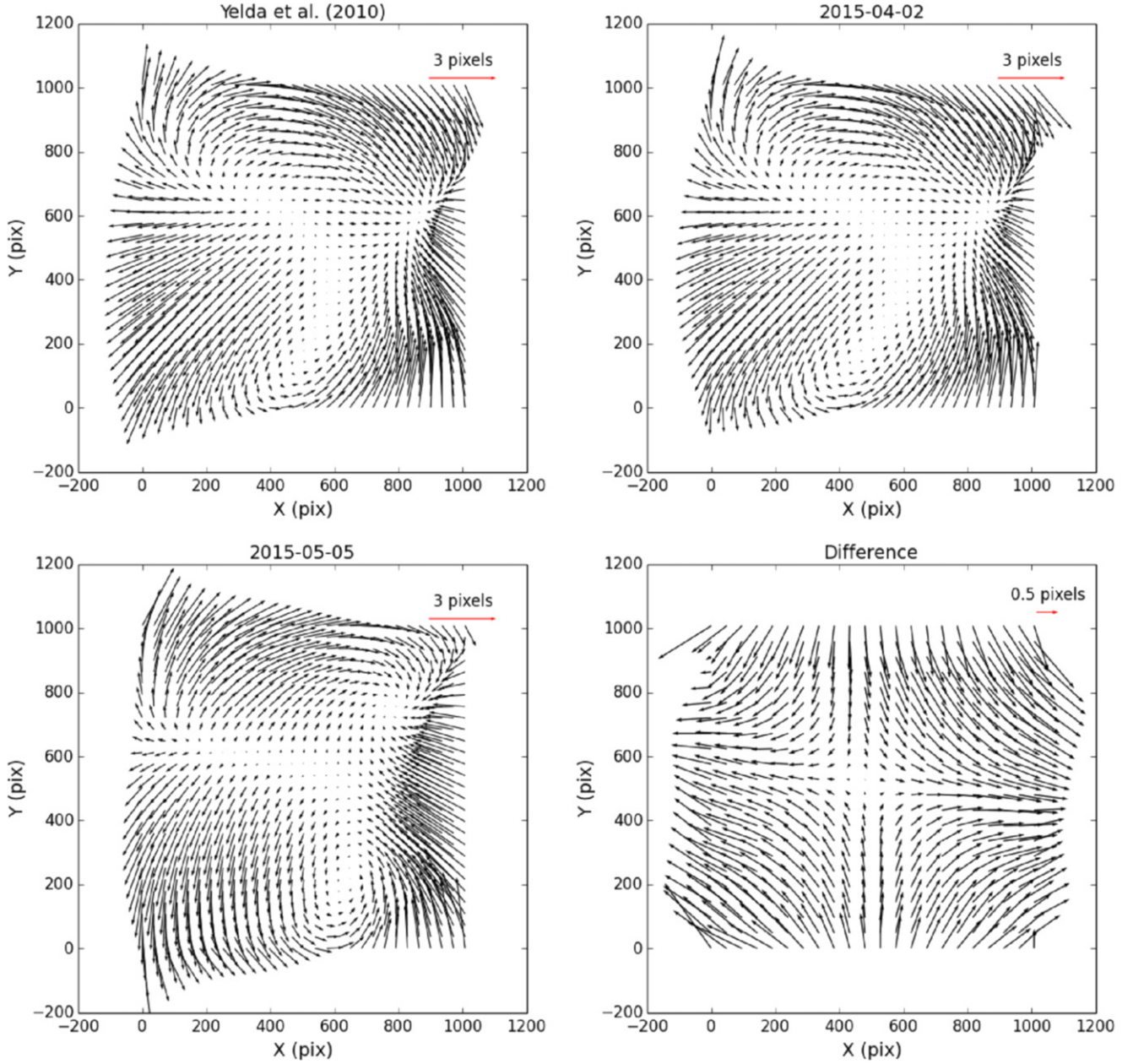
Figure 8. Top: distortion models for the pre-realignment NIRC2 system. Arrows show the X and Y values that must be added to cancel the effects of geometric distortion. (left) The solution previously published in Yelda et al. (2010) and (right) the solution derived using the methodology of this work. It is evident that these two are very similar and are, in fact, statistically equivalent. Bottom left: distortion model derived from the May observations. Bottom right: change of the optical distortion as a result of the optical realignment. This is the difference between the 2015-05-05 solution and the solution derived in Yelda et al. (2010). The average absolute value of the residual difference is ∼4.5 mas.
(A color version of this figure is available in the online journal.)

plate scale and orientation in each data epoch (Table 2), as theses parameters were already fit to transform the coordinates. We estimate the scale and position angle relative to the *HST* reference frame for each of the distortion-corrected NIRC2 image and average the results. This yields a global plate scale

$\langle s \rangle = 9.971 \pm .004 \pm .001$ mas pixel^{-1} post-realignment and $\langle s \rangle = 9.952 \pm .002 \pm .001$ mas pixel^{-1} pre-realignment. The first error is the rms of the measurements from the individual images and the second are the errors in the *HST*/ACS absolute reference frame (van der Marel et al. 2007).
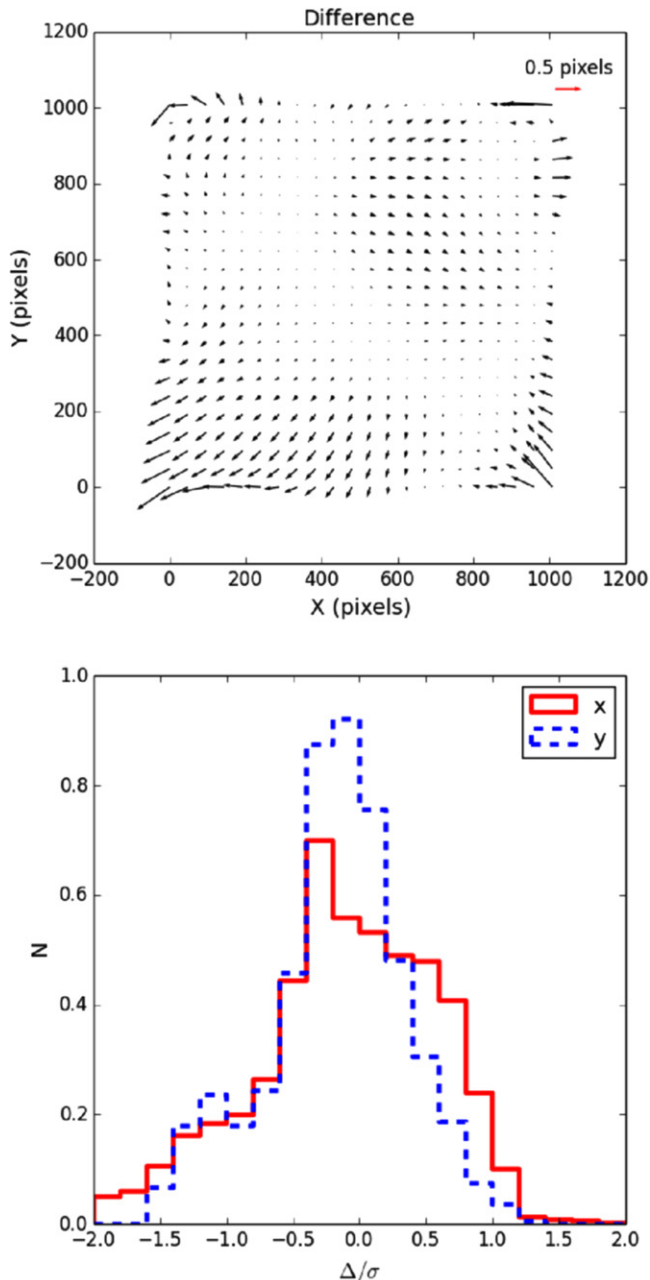
Figure 9. Difference between the previous solution (Yelda et al. 2010) and the pre-realignment 2015-04-02 solution from this work. The map of the vector differences (top) show the two solutions are consistent within 1 mas over most of the field of view. Larger differences are seen in the corners. The distribution of differences normalized by the errors in each distortion solution is also shown (bottom). Errors include the fitting errors (Figure 7) and the 1.0 mas additive term describing the residual distortion for both solutions. While the distribution is not exactly Gaussian, more than 90% of the differences are within the 1σ (~1.4 mas) measurement errors.

(A color version of this figure is available in the online journal.)

Table 2
NIRC2 Plate Scale and Orientation

Data	Plate Scale (mas pixel^{-1})	Orientation (degrees)
Yelda et al. (2010)	9.952 ± 0.002	0.252 ± 0.009
M53—April	$9.954 \pm 0.002 \pm 0.001$	$0.245 \pm 0.018 \pm 0.002$
M53—May	$9.971 \pm 0.004 \pm 0.001$	$0.262 \pm 0.020 \pm 0.002$

5.4. Using the New Distortion Solution

Both the solutions and their associated errors are publicly available from the NIRC2 webpage[6]. The lookup tables present the distortion at the center of each NIRC2 pixel as well as the associated errors. This can be applied using existing programs (e.g., *Drizzle*) to correct distortion in NIRC2 data taken after 2015 April 13.

6. Summary

We have derived a new model for the geometric distortion in observations obtained with the Keck NIRC2 narrow camera after 2015 April 13, when the optical system was realigned. The techniques used build on those of Yelda et al. (2010), with the primary advantage being a more robust basis set when fitting the distortion parameters and improved data quality. We verified that these technical differences do not significantly affect the derived models and that we can recover the optical distortion of the system, pre-realignment, using the modified technique on a new data set. The Yelda et al. (2010) distortion solution should still be used for all pre-realignment data for the sake of consistency, as the pre-realignment solution from this work is statistically equivalent. The new post-realignment distortion solution (2015-05-05) should be used for all observations taken after 2015 April 13. The 2015-05-05 distortion solution along with associated errors are made publicly available (see footnote 6), to assist with other astrometric projects using NIRC2. The systematic error in the new solution is dominated by the use of a single PSF for the entire field of view despite the fact it varies due to anisoplanatism and field-dependent wavefront error. This shortcoming will be addressed in future work using this data set, with the primary advancement being the application of a spatially varying PSF in the position extraction from the individual science frames.

---

[6] https://www2.keck.hawaii.edu/inst/nirc2/dewarp.html

wish to recognize and acknowledge the very significant cultural role and reverence that the summit of Mauna Kea has always had within the indigenous Hawaiian community. We are most fortunate to have the opportunity to conduct observations from this mountain.

References

Anderson, J. 2007, Variation of the Distortion Solution of the WFC, Tech. Rep.
Anderson, J., & King, I. R. 2006, PSFs, Photometry, and Astronomy for the ACS/WFC, Tech. Rep.
Anderson, J., Sarajedini, A., Bedin, L. R., et al. 2008, AJ, 135, 2055
Bartko, H., Martins, F., Fritz, T. K., et al. 2009, ApJ, 697, 1741
Cameron, P. B., & Kulkarni, S. R. 2007a, BAAS, 39, 996
Cameron, P. B., & Kulkarni, S. R. 2007b, ApJ, 665, L135
Clarkson, W. I., Ghez, A. M., Morris, M. R., et al. 2012, ApJ, 751, 132
De Rosa, R. J., Nielsen, E. L., Blunt, S. C., et al. 2015, ApJl, 814, L3
Diolaiti, E., Bendinelli, O., Bonaccini, D., et al. 2000, A&AS, 147, 335
Dupuy, T. J., Liu, M. C., & Ireland, M. J. 2014, ApJ, 790, 133
Eckart, A., & Genzel, R. 1997, MNRAS, 284, 576
Fruchter, A. S., & Hook, R. N. 2002, PASP, 114, 144
Genzel, R., Schödel, R., Ott, T., et al. 2003, ApJ, 594, 812
Ghez, A. M., Klein, B. L., Morris, M., & Becklin, E. E. 1998, ApJ, 509, 678
Ghez, A. M., Salim, S., Hornstein, S. D., et al. 2005, ApJ, 620, 744
Grundy, W. M., Porter, S. B., Benecchi, S. D., et al. 2015, Icar, 257, 130
Gubler, J., & Tytler, D. 1998, PASP, 110, 738
Kharchenko, N. V., Piskunov, A. E., Schilbach, E., Röser, S., & Scholz, R.-D. 2013, A&A, 558, A53
Kimmig, B., Seth, A., Ivans, I. I., et al. 2015, AJ, 149, 53
Konopacky, Q. M., Ghez, A. M., Duchêne, G., McCabe, C., & Macintosh, B. A. 2007, AJ, 133, 2008
Liu, M. C., Dupuy, T. J., & Ireland, M. J. 2008, ApJ, 689, 436
Lu, J. R. 2008, PhD thesis, Univ. California, Los Angeles
Lu, J. R., Ghez, A. M., Hornstein, S. D., et al. 2009, ApJ, 690, 1463
Meyer, L., Ghez, A. M., Schödel, R., et al. 2012, Sci, 338, 84
Paumard, T., Genzel, R., Martins, F., et al. 2006, ApJ, 643, 1011
Pueyo, L., Soummer, R., Hoffmann, J., et al. 2015, ApJ, 803, 31
Rudy, A., Horns, D., DeLuca, A., et al. 2015, ApJ, 811, 24
Stolte, A., Ghez, A. M., Morris, M., et al. 2008, ApJ, 675, 1278
van der Marel, R. P., Anderson, J., Cox, C., et al. 2007, Calibration of ACS/WFC Absolute Scale and Rotation for Use in creation of a JWST Astrometric Reference Field, Tech. Rep.
Yelda, S., Ghez, A. M., Lu, J. R., et al. 2014, ApJ, 783, 131
Yelda, S., Lu, J. R., Ghez, A. M., et al. 2010, ApJ, 725, 331